Clusters

Luca Di Stasio[a], Janis Varna[a]

[a] *Luleå University of Technology, University Campus, SE-97187 Luleå, Sweden*

Abstract

Keywords: Polymer-matrix Composites (PMCs), Transverse Failure, Debonding, Finite Element Analysis (FEA)

1. Introduction

2. RVE models & FE discretization

2.1. Introduction & Nomenclature

2.2. Models of Representative Volume Element (RVE) and equivalent boundary conditions

2.3. Finite Element (FE) discretization

Discretization and analysis of RUCs is performed with the Finite Element Method (FEM) within the Abaqus environment, a commercial FEM software [1]. Length l and height h of the model are respectively determined by the number of fibers n in the horizontal direction and k across the thickness (see Sec. 2.2) according to Eq. 1:

$$l = 2nL \qquad h = kL; \tag{1}$$

where $2L$ is the length of a one-fiber unit, see Fig. 2, and L is defined as a function of the fiber volume fraction V_f and the fiber radius R_f according to

$$L = \frac{R_f}{2}\sqrt{\frac{\pi}{V_f}}. \tag{2}$$

R_f is assumed to be the same for every fiber and equal to 1 μm. The choice of the previous value is not dictated by physical considerations but for

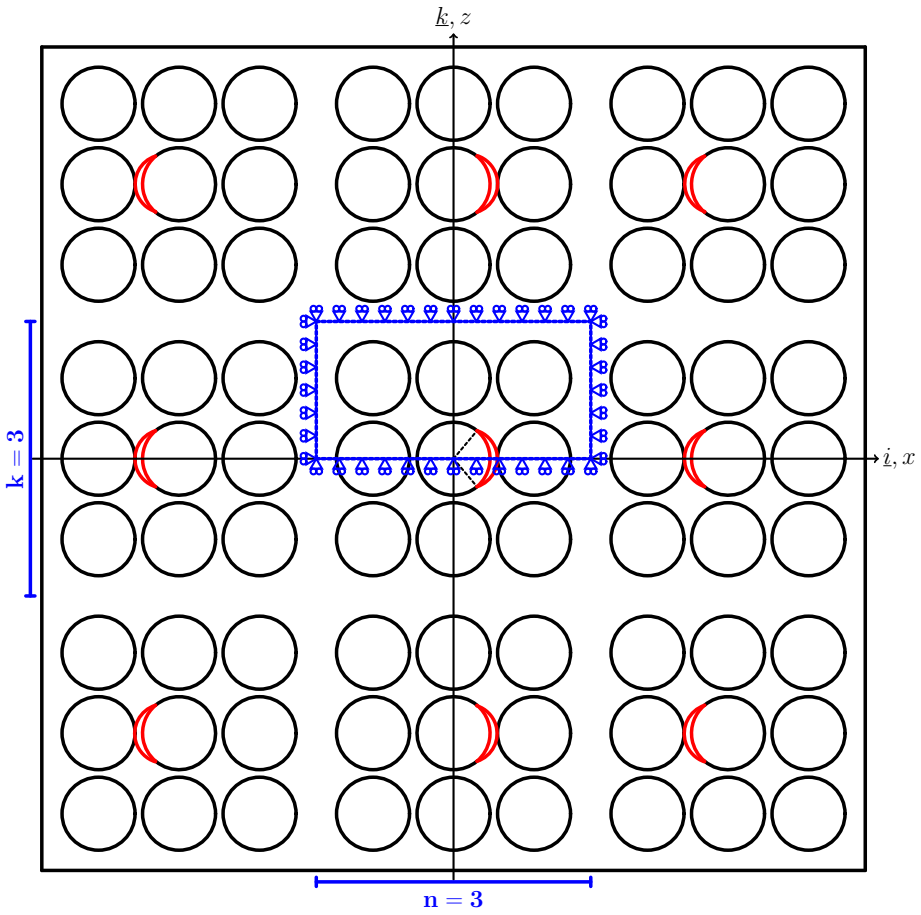

Figure 1: Models $n \times k -$ *coupling* with clusters.

simplicity. It is thus useful to remark here that, in a linear elastic solution as the one considered in the present work, the ERR is proportional to the geometrical dimensions of the model and, consequently, recalculation of the ERR for fibers of any size requires a simple multiplication. Notice also that relationships in Eqs. 1 and 2 imply that the local and global V_f are everywhere equal.

The debond is placed symmetrically with respect to the x axis (see Fig. 2) and it is characterized by an angular size of $\Delta\theta$ (making the full debond size equal to $2\Delta\theta$). For large debond sizes (at least $\geq 60° - 80°$), a region $\Delta\Phi$ of variable size appears at the crack tip where the crack faces are in contact with

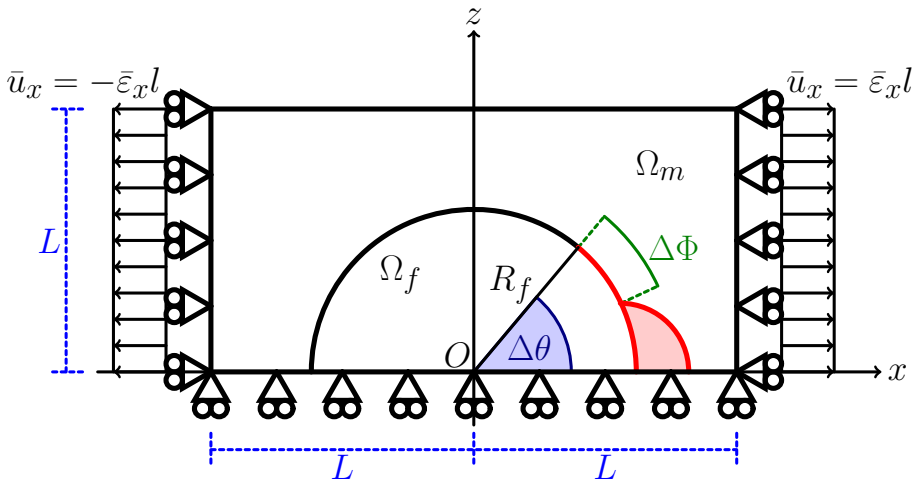

Figure 2: Schematic of the model with its main parameters.

each other but free to slide relatively to each other. In order to model crack faces motion in the contact zone, frictionless contact is considered between the two crack faces to allow free sliding and avoid interpenetration. Symmetry with respect to the x axis is applied on the lower boundary and coupling of vertical displacement on the upper boundary. Kinematic coupling on the x-displacement is applied along the left and right sides of the RUC in the form of a constant x-displacement $\pm\bar{\varepsilon}_x l$, corresponding to transverse strain $\bar{\varepsilon}_x$ equal to 1%.

Table 1: Summary of the mechanical properties of fiber and matrix. E stands for Young's modulus, μ for shear modulus and ν for Poisson's ratio.

Material	$E\,[GPa]$	$\mu\,[GPa]$	$\nu\,[-]$
Glass fiber	70.0	29.2	0.2
Epoxy	3.5	1.25	0.4

Meshing of the model is accomplished with second order, 2D, plane strain triangular (CPE6) and quadrilateral (CPE8) elements. A regular mesh of 8-node (2^{nd} order rectangular) elements with almost unitary aspect ratio is enforced at the crack tip in order to ensure the convergence of the ERR. The angular size

δ of an element in the crack tip neighborhood is always equal to 0.05°. The crack faces are modeled as element-based surfaces and a small-sliding contact pair interaction with no friction is imposed between them. The Mode I, Mode II and total Energy Release Rates (ERRs) (respectively referred to as G_I, G_{II} and G_{TOT}) are the main result of FEM simulations; they are evaluated using the VCCT [2] implemented in a in-house Python routine and, for G_{TOT} only, the J-integral [3] is calculated by use of the Abaqus built-in command. A glass fiber-epoxy UD composite is treated in the present work, and it is assumed that their response lies always in the linear elastic domain. The material properties of glass fiber and epoxy are reported in Table 1. Validation is performed with respect to the results reported in [4, 5], which were obtained with the Boundary Element Method (BEM) for a model of a single fiber with a symmetric debond placed in an infinite matrix. As discussed in more detail in [6], the agreement between FEM (present work) and BEM [4, 5] solutions is good and the difference between the two does not exceed 5%. This provides us with a level of uncertainty with which we can analyze the significance of observed trends: any relative difference in ERR between different RUCs smaller than 5% cannot be reliably distinguished from numerical uncertainty and its discussion should thus be avoided.

3. Results & Discussion

3.1. Coupling

3.2. Cross-ply

4. Conclusions & Outlook

Acknowledgements

References

[1] Simulia, Providence, RI, USA, ABAQUS/Standard User's Manual, Version 6.12 (2012).

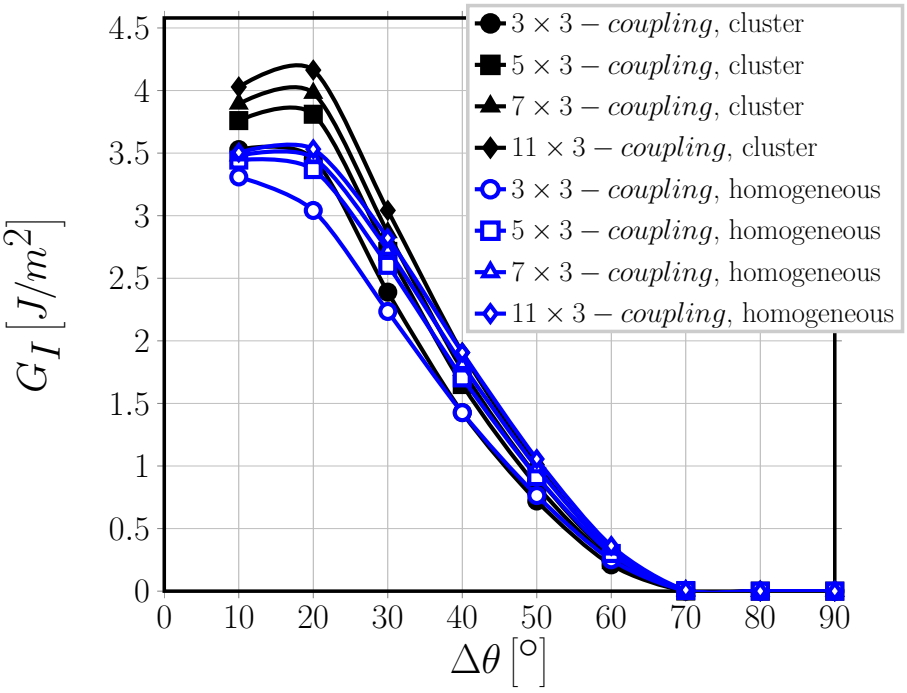

Figure 3: Clustering: models $n \times 1 - coupling$. $V_f = 60\%$, $\varepsilon_x = 1\%$.

[2] R. Krueger, Virtual crack closure technique: History, approach, and applications, Applied Mechanics Reviews 57 (2) (2004) 109. doi:10.1115/1.1595677.

[3] J. R. Rice, A path independent integral and the approximate analysis of strain concentration by notches and cracks, Journal of Applied Mechanics 35 (2) (1968) 379. doi:10.1115/1.3601206.

[4] F. París, E. Correa, V. Mantič, Kinking of transversal interface cracks between fiber and matrix, Journal of Applied Mechanics 74 (4) (2007) 703. doi:10.1115/1.2711220.

[5] C. Sandino, E. Correa, F. París, Numerical analysis of the influence of a nearby fibre on the interface crack growth in composites under transverse tensile load, Engineering Fracture Mechanics 168 (2016) 58–75. doi:10.1016/j.engfracmech.2016.01.022.

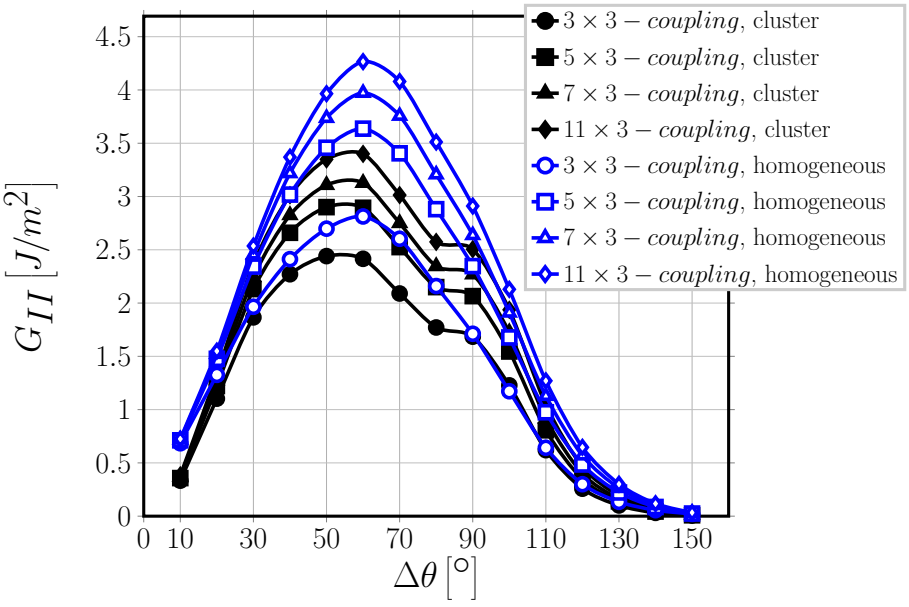

Figure 4: Clustering: models $n \times 1 - coupling$. $V_f = 60\%$, $\varepsilon_x = 1\%$.

[6] L. Di Stasio, J. Varna, Z. Ayadi, Energy release rate of the fiber/matrix interface crack in UD composites under transverse loading: effect of the fiber volume fraction and of the distance to the free surface and to non-adjacent debonds, Theoretical and Applied Fracture Mechanics (2019) 102251doi: 10.1016/j.tafmec.2019.102251.

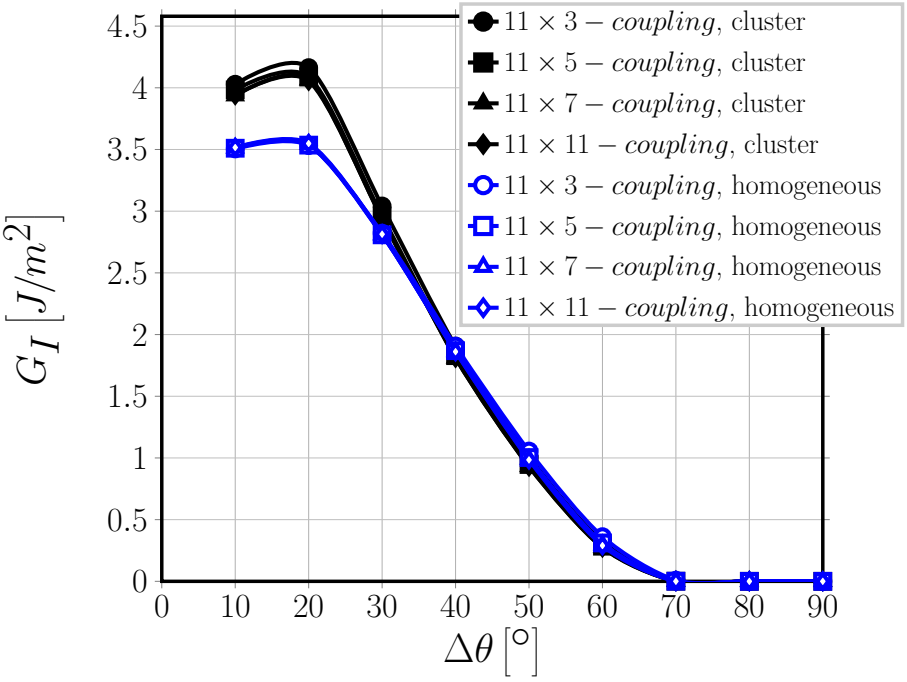

Figure 5: Clustering: models $11 \times k - coupling$. $V_f = 60\%$, $\varepsilon_x = 1\%$.

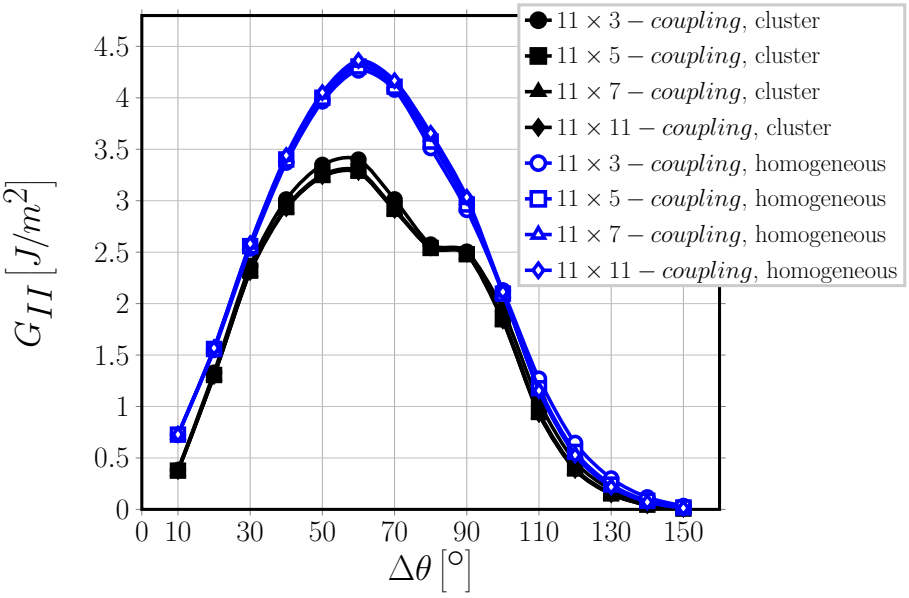

Figure 6: Clustering: models $11 \times k - coupling$. $V_f = 60\%$, $\varepsilon_x = 1\%$.

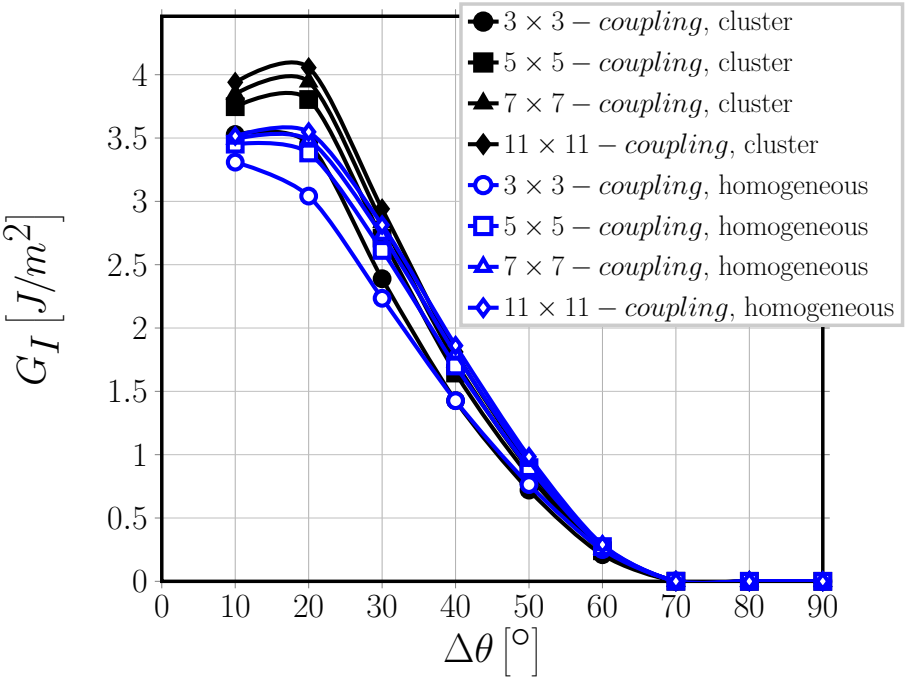

Figure 7: Clustering: models $n \times n - coupling$. $V_f = 60\%$, $\varepsilon_x = 1\%$.

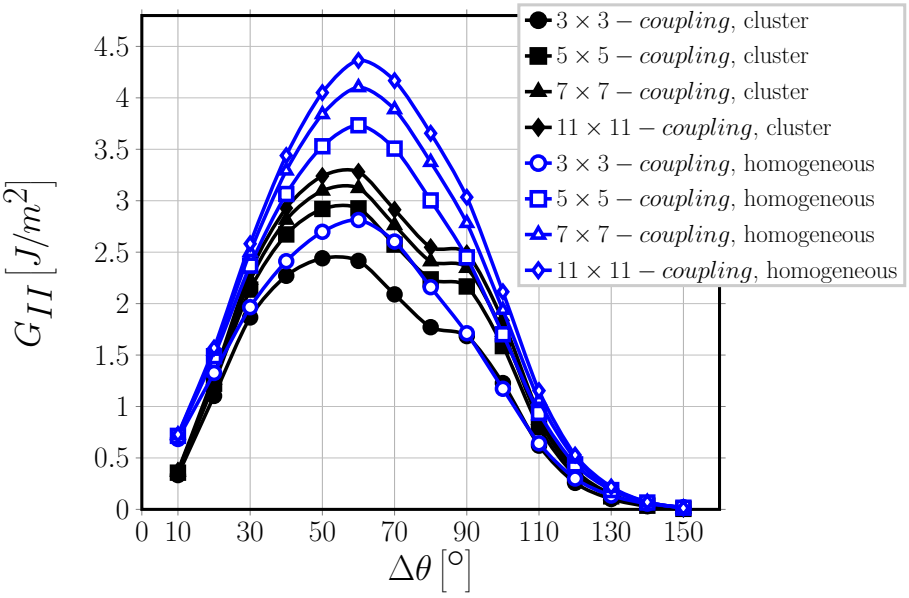

Figure 8: Clustering: models $n \times n - coupling$. $V_f = 60\%$, $\varepsilon_x = 1\%$.

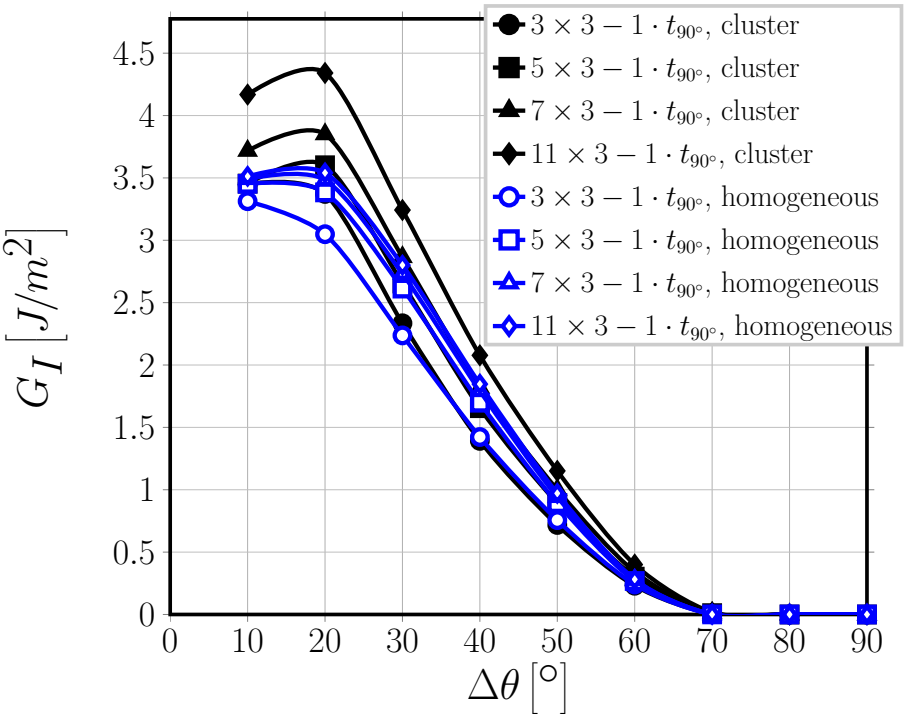

Figure 9: Clustering: models $n \times 1 - 1 \cdot t_{90^\circ}$. $V_f = 60\%$, $\varepsilon_x = 1\%$.

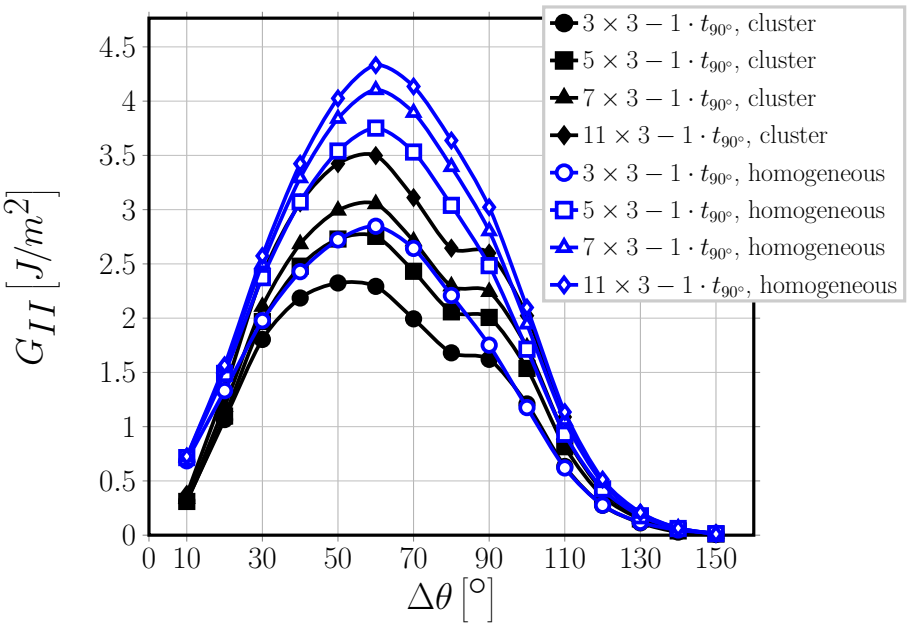

Figure 10: Clustering: models $n \times 1 - 1 \cdot t_{90^\circ}$. $V_f = 60\%$, $\varepsilon_x = 1\%$.

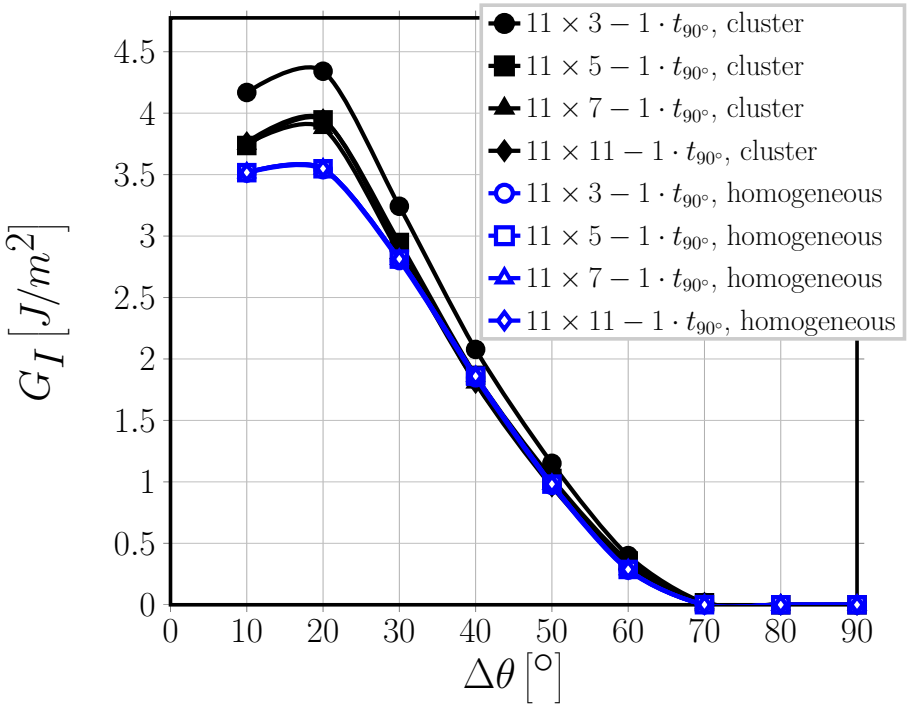

Figure 11: Clustering: models $11 \times k - 1 \cdot t_{90^\circ}$. $V_f = 60\%$, $\varepsilon_x = 1\%$.

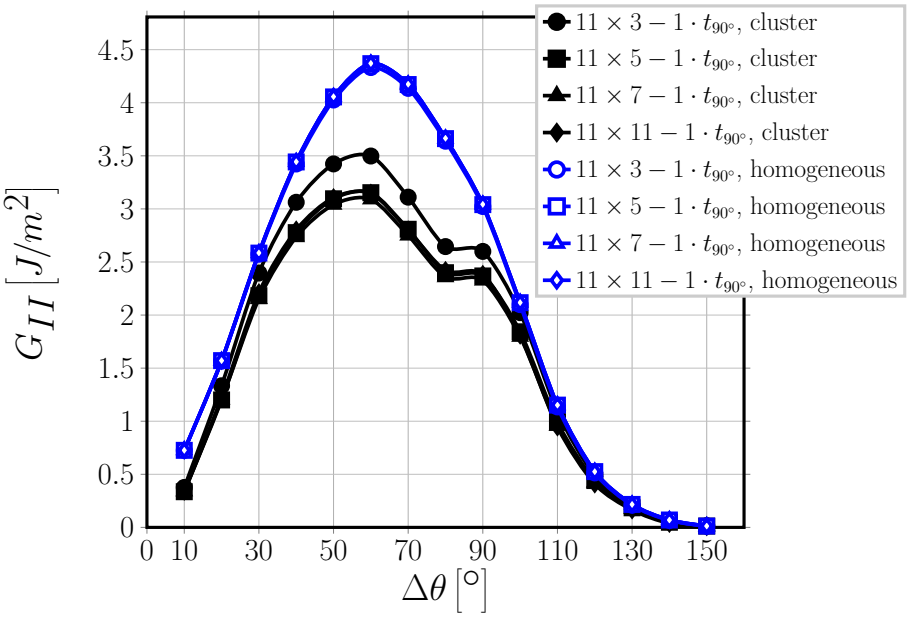

Figure 12: Clustering: models $11 \times k - 1 \cdot t_{90^\circ}$. $V_f = 60\%$, $\varepsilon_x = 1\%$.

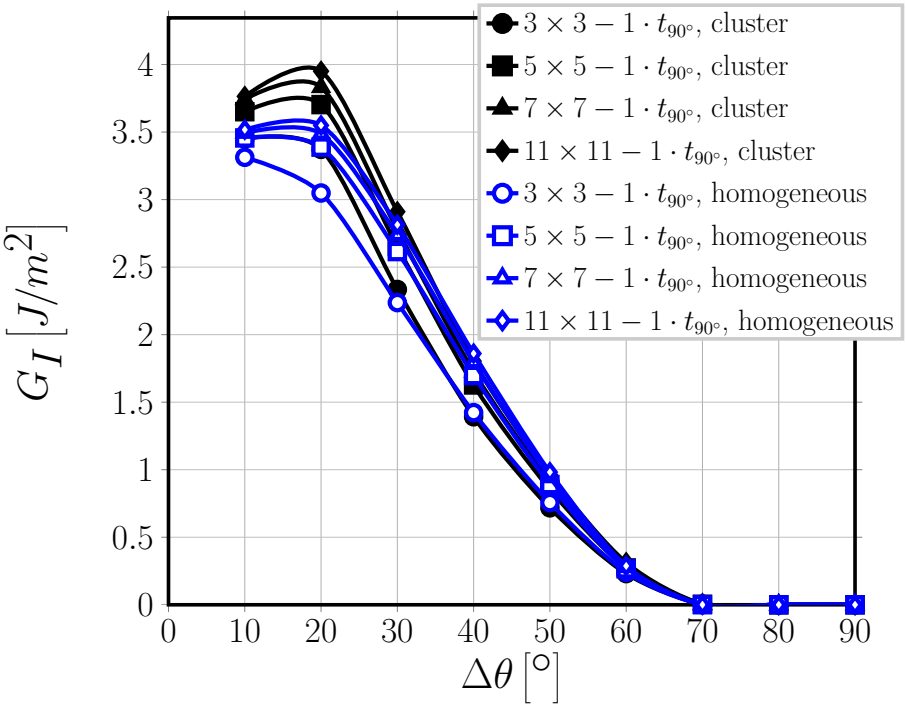

Figure 13: Clustering: models $n \times n - 1 \cdot t_{90^\circ}$. $V_f = 60\%$, $\varepsilon_x = 1\%$.

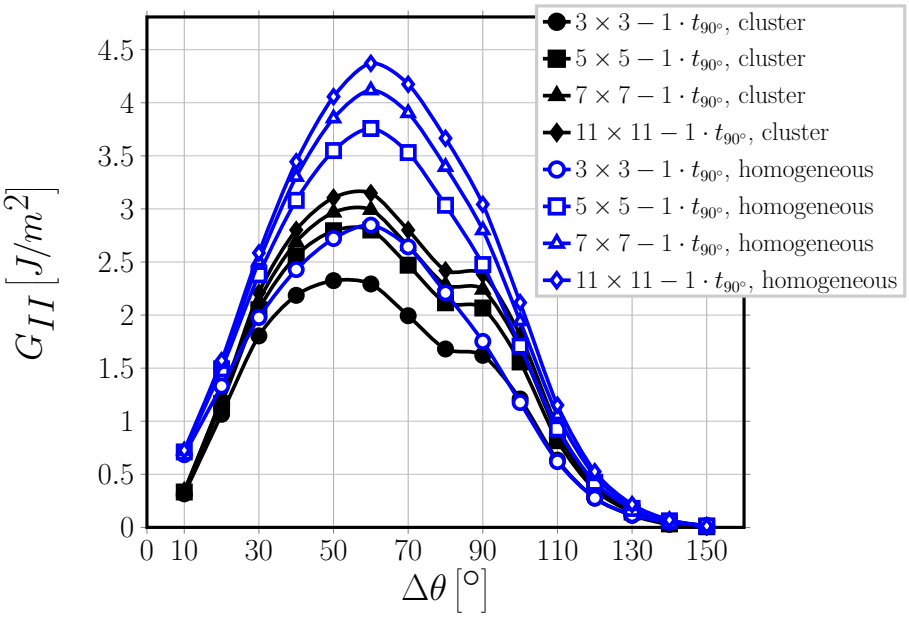

Figure 14: Clustering: models $n \times n - 1 \cdot t_{90^\circ}$. $V_f = 60\%$, $\varepsilon_x = 1\%$.